ACS OMEGA

http://pubs.acs.org/journal/acsodf

Article

Roles of HNO_x and Carboxylic Acids in the Thermal Stability of Nitroplasticizer

Kitmin Chen, Alexander S. Edgar, Zheng-Hua Li, Oana C. Marina, and Dali Yang*

Cite This: *ACS Omega* 2023, 8, 14730−14741

Read Online

ACCESS | Metrics & More | Article Recommendations | Supporting Information

ABSTRACT: In the thermal aging of nitroplasticizer (NP), the produced nitrous acid (HONO) can decompose into reactive nitro-oxide species and nitric acid (HNO_3). These volatile species are prone to cause cascaded deterioration of NP and give rise to various acidic constituents. To gain insight on the early stage of NP degradation, an adequate method for measuring changes in the concentrations of HONO, HNO_3, and related acidic species is imperative. The typical assessment of acidity in nonaqueous solutions (i.e., acid number) cannot differentiate acidic species and thus presents difficulty in the measurement of HONO and HNO_3 at a micromolar concentration level. Using liquid−liquid extraction and ion chromatography (IC), we developed a fast and unambiguous analytical method to accurately determine the concentration of HONO, HNO_3, acetic/formic acids, and oxalic acid in aged NP samples. Given by the overlay analysis results of liquid chromatography coupled with quadrupole time-of-flight mass spectrometry and IC, the prominent increase of produced HONO after the depletion of antioxidants is the primary cause of HNO_3 formation in the late stage of NP degradation, which results in the acid-catalyzed hydrolysis of NP into 2,2-dinitropropanol and acetic/formic acids. Our study has demonstrated that the aging temperature plays a crucial role in accelerating the formation and decomposition of HONO, which consequently increases the acidity of aged NP samples and hence accelerates the hydrolyzation of NP. Therefore, to prevent NP from undergoing rapid degradation, we suggest that the concentration of HNO_3 should be maintained below 1.35 mM and the temperature under 38 °C.

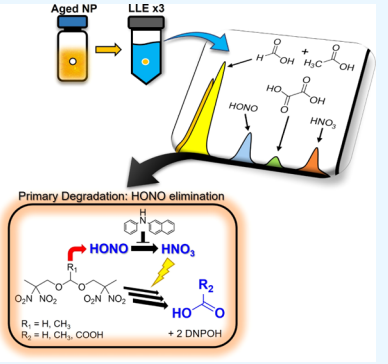

1. INTRODUCTION

The formation of acidic constituents is a critical threat to the long-term stability of fuels, polymers, and plasticizers.[1−3] Particularly for the eutectic bis(2,2-dinitropropyl) acetal/formal (BDNPA/F) liquid mixture, hereinafter referred to as nitroplasticizer (NP), as a binder component, its stability can directly affect the properties of energetic composites. At moderate temperatures (<55 °C), nitrous acid (HONO) elimination (via intramolecular hydrogen transfer to the nearby NO_2 moiety) is hypothesized as the initial degradation reaction of NP (Figure S1).[4,5] It is commonly known that HONO is unstable in nature; thus, the fate of the produced HONO from NP is subject to decomposition. As displayed in reaction 1, HONO decomposition produces water and reactive nitro-oxide species, such as nitrogen monoxide ($NO^\bullet$) and dioxide ($NO_2^\bullet$).

$$2HONO \rightarrow NO^\bullet + NO_2^\bullet + H_2O \quad (1)$$

Through the plausible reactions 2) to 5),[6−12] the free radicals can subsequently generate other volatile products. In the 2008 constituent aging study, the concentration profiles of $NO^\bullet$, N_2O, CO, and CO_2 gas products were extracted and found to be associated with NP decomposition.[13] Through reactions 1, (3), and (5), $NO^\bullet$ and N_2O will form. As for carbon oxides (CO_x), it is believed that they can be produced from the oxidation and chain scission reactions of NP.[5,14] Among all decomposed products of HONO, the combination of nitric acid (HNO_3) and water is particularly harmful to the stability of NP due to acid-catalyzed hydrolysis. Therefore, it is important to understand when and how HONO and HNO_3 are generated in NP degradation.

$$2NO_2^\bullet + H_2O \rightleftharpoons HNO_3 + HONO \quad (2)$$

$$4NO^\bullet \rightarrow 2N_2O + O_2 \quad (3)$$

$$2NO^\bullet + O_2 \rightarrow 2NO_2^\bullet \quad (4)$$

$$4HONO \rightarrow N_2O + H_2O + 2HNO_3 \quad (5)$$

To address the effect of HONO decomposition on NP degradation, a nitration pathway of the antioxidant *n*-phenyl-*β*-naphthylamine (PBNA) established in the previous study must be revisited.[15] As proposed in Scheme 1, the reactions between PBNA (**1a**), NP (**1b**), and the key volatile products ($NO_2^\bullet$,

Received: February 5, 2023
Accepted: March 28, 2023
Published: April 11, 2023

Scheme 1. Proposed Time Evolution of Degradation in NP Components[a]

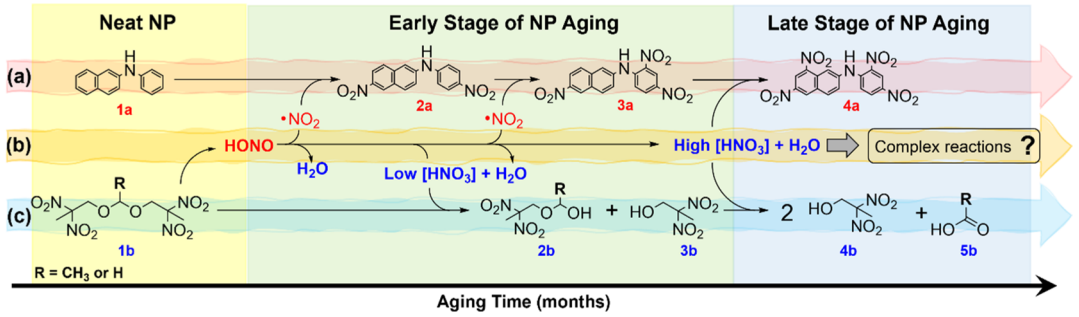

[a]Three parallel reaction pathways and their corresponding products are proposed to demonstrate their interactions with one another from the early to the late stage of NP aging: (a) By scavenging $NO_2^{\bullet}$ (or NO_2^+), nitration of PBNA (**1a**) forms dinitro- (**2a**), trinitro- (**3a**), and tetra-nitro- (**4a**) PBNA derivatives; (b) HONO are initially produced from the elimination reaction via the intramolecular hydrogen transfer to the nearby NO_2 moiety in NP, which can be further decomposed into $NO_2^{\bullet}$, HNO_3, water, and other volatile species. In further progression, the high abundance of these reactive small molecules will result in complex reactions. (c) From the produced HNO_3, NP can be hydrolyzed into hemiacetal/hemiformal (**2b**), DNPOH (**3b** and **4b**), and aldehyde products, which are then oxidized into organic acids (acetic/formic acids, **5b**).

Scheme 2. Mechanism of Acid-Catalyzed Acetal/formal and Hemiacetal/Hemiformal Hydrolyses and Nitric Acid Oxidation

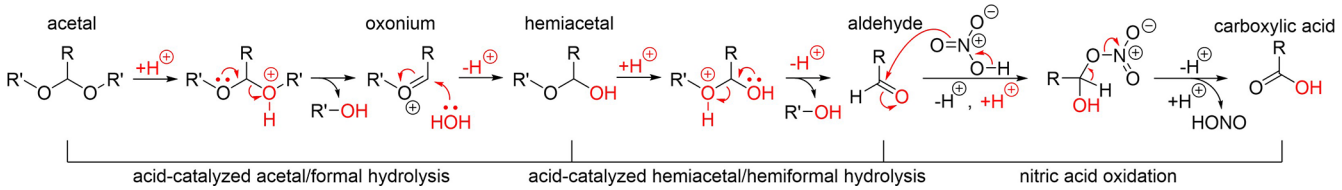

NO_2^+, and HNO_3) can generate a suite of degraded products from NP. There are three degradation routes which progress synchronously and dynamically as a function of time: (a) PBNA nitration, (b) HONO formation and decomposition, and (c) NP hydrolysis (detailed mechanism as shown in Scheme 2). In the early stage, since the produced $NO_2^{\bullet}$ from HONO decomposition is scavenged by PBNA, the formation of HNO_3 (i.e., reaction 2) is minimized.[15,16] As the number of its NO_2 moieties increases, the scavenging efficiency of PBNA decreases. Among the identified PBNA nitro derivatives, dinitro-PBNA (**2a**) is the last derivative that remains effective in scavenging $NO_2^{\bullet}$, whereas trinitro-PBNA (**3a**) is the nullified (less effective) form of this antioxidant.[15,16] Consequently, HNO_3 starts to form at a slow rate. At low acidity and due to the electron density being drawn away by the nitro groups, the protonation of acetal/formal oxygen in NP is destabilized (Scheme 2). Therefore, the acetal/formal hydrolysis of NP proceeds at a slow or negligible rate at low temperatures (≤45 °C) in the early aging stage. When the HNO_3 concentration reaches the threshold of 1.35 mM, which is capable of stabilizing the protonated form of acetal/formal oxygen in NP, NP can undergo nucleophilic addition of water to first form 2,2-dinitropropanol (DNPOH, **3b**) and an oxonium ion, which then produce the hemiacetal/hemiformal (Scheme 1, **2b**) in the latter water addition (Scheme 2).[17−20] Moreover, the localized clusters or microdroplets of produced water can promote an interfacial nitration reaction in the presence of HNO_3 and volatiles (e.g., NO_2^+),[21−23] which accelerates PBNA depletion. This early-stage process is described as a partial hydrolysis of NP.

Our previous study of PBNA nitration also demonstrates that the formation of tetra-nitro-PBNA (Scheme 1, **4a**) is an indication of high acidity, which is followed by the depletion of dinitro-PBNA.[15] Here, we define it as the late stage of NP aging. In the presence of trinitro-PBNA, the formation of HNO_3 will no longer be suppressed. Subsequently, the acidity of the aged NP samples increases, which accelerates the acetal/formal and hemiacetal/hemiformal hydrolyses of NP at a rapid rate. Therefore, the NP is projected to fully decompose into DNPOH (**4b**) and aldehydes (Scheme 2). Surrounded by HNO_3 and water, aldehydes can be oxidized to organic acids (e.g., acetic and formic acids, **5b**).[17−20] In a highly acidic environment, the hemiacetal/hemiformal is expected to only exist as a transient intermediate. Additionally, CO_2 and CO can be converted into oxalic acid: (1) a coupling product of CO_2 that is promoted by the energy storage of C−C bond formation ($2CO_2 + 2e^- \rightarrow C_2O_4^{2-}$);[24] (2) a dialkyl oxalate product of the reaction between an alcohol (i.e., DNPOH) and CO, which is then hydrolyzed into oxalic acid, as shown in Scheme 3.[25]

Scheme 3. Plausible Reaction of Oxalic Acid Formation

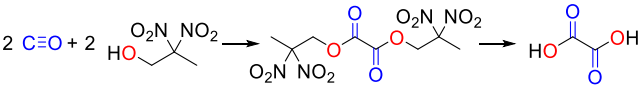

Based on the time−temperature superposition (TTS) principle, while maintaining the same degradation profile, the three parallel reaction pathways in Scheme 1 are expected to be significantly faster at elevated temperatures (≥55 °C). However, the potentially high abundance of reactive small molecules in the late stage of NP aging, such as $NO_2^{\bullet}$ and HNO_3, can alter and further complicate the overall mechanism. For instance, the decomposition of HNO_3 via reactions 6 and (7) may occur, and the $NO_2^{\bullet}$ radicals are also free to abstract the hydrogen atoms from neighboring NP, as shown in reaction 8.[14]

https://doi.org/10.1021/acsomega.3c00748
ACS Omega 2023, 8, 14730−14741

$$4HNO_3 \overset{\text{heat}}{\rightleftharpoons} 4NO_2^{\bullet} + 2H_2O + O_2 \quad (6)$$

$$HNO_3 + 2NO^{\bullet} + H_2O \rightleftharpoons 3HONO \quad (7)$$

$$NO_2^{\bullet} + NP \rightarrow HONO + [NP^{\bullet}\text{-}H] \quad (8)$$

It has been demonstrated that water can effectively inhibit the thermal decomposition of HNO_3 at high temperatures (<88 °C) in reaction 6.[12] Therefore, aging NP in direct contact with water may present a significant difference from that in ordinary storage conditions (<38 °C, sealed in air). Moreover, it was reported that $NO^{\bullet}$ is formed during the early stage and consumed in the late stage of NP aging at 64 °C.[13] Perhaps, $NO^{\bullet}$ gas is another contribution that influences the dynamic between HONO and HNO_3 (reaction 7). Hence, the reported concentration profiles of $NO^{\bullet}$ in NP aging may help draw the connection between HNO_3 decomposition and the proposed pathways in Scheme 1.[13] Apparently, the above reactions are all related to the formation and consumption of acidic molecules in the aging process of the NP. To examine these plausible mechanisms, an analytical method to obtain acid profiles of aged NP is needed.

To probe the general behaviors of degradation products in NP aging, we referred to their physical and chemical properties, as listed in Table 1. The different densities and solubilities in these chemicals may result in phase partitioning in the NP phase over time, meaning that the acidic constituents can be deposited in localized water clusters,[22,23] whereas the high density and low solubility products, such as DNPOH, can sink to the bottom of the NP phase.

Table 1. Physical and Chemical Properties[a]

	molecular weight (g/mol)	density at 20−25 °C (g/cm^3)	pK_a[26]	water solubility rating
BDNPA/F	326.23/312.23	1.392	N/A	insoluble
DNPOH	150.09	1.483	N/A	minimal
HONO	47.01	N/A	3.29	minimal[10]
HNO_3 (15.7 M)	63.01	1.413	−1.3	soluble
acetic acid	60.05	1.049	4.76	soluble
formic acid	46.03	1.22	3.77	soluble
oxalic acid	90.03	1.9	1.23/4.19	soluble

[a]Data are obtained from available SDS.

Regarding the displacement of these chemicals, HONO exhibits high volatility and poor water solubility, although its pK_a is 3.29, which suggests that the decomposition reaction 1 and the potential loss of HONO by evaporation to the vapor phase are preferable when there is some available headspace (including microvoids and bubbles in a heterogeneous matrix). Therefore, the quantitation of HONO will be less accurate than other more stable molecules, such as HNO_3 and DNPOH. Based on their pK_a values, HNO_3 is the strongest acid among all acidic constituents (pK_a −1.3). Therefore, HNO_3 is theorized as the key catalyst that facilitates the hydrolyzation of NP. Furthermore, the acidity on the surface of localized water clusters can be enhanced (lower pK_a) by the deposited carboxylic acids, which subsequently changes the uptake of chemicals.[27] For example, the interfacial acetic acid can exhibit strong-acid-like and amphiphilic-like properties because in the NP−water interface, its −COOH group is oriented inward to the hydrophilic core (aqueous phase), and its $-CH_3$ group is displaced outward on the hydrophobic layer (NP phase).[27] As the aging time increases, the increased acidity at the NP−water interface can ultimately change the water solubility of NP from insoluble to soluble.

Conventionally, an acid number (AN) titration method (via NaOH or KOH) has been utilized to assess the acidity of nonaqueous solutions, which is measured as the sum of all acidic species.[1,2] However, it requires a large sample size (up to 50 mL) and does not provide specific profiles of the acid molecules, which has presented major challenges to engage in the study of early NP degradation. In this work, a fast and direct methodology is developed to determine the concentrations of HONO, HNO_3, acetic/formic acids, and oxalic acid at micromolar levels (μM or μmol/L NP), which allows us to investigate their roles in controlling and dictating reaction pathways in NP degradation. This methodology involves a simple liquid−liquid extraction (LLE) of sample size in milligrams and analysis by ion chromatography (IC).

2. RESULTS AND DISCUSSION

2.1. Conversion of HONO to HNO_3. In Figure 1, the control experiment shows low concentrations of HNO_3 (<2.2 weight percent or wt %) are detected in all HONO solutions (a), whereas HONO is not detected in all HNO_3 solutions (b), confirming that HONO can be converted to HNO_3 at ambient temperature but not vice versa. This conversion is mainly caused by the unstable characteristic of HONO, which can be achieved by reactions 1 and (2).[10] Yet again, this observation can only be applied to low-temperature environments. As

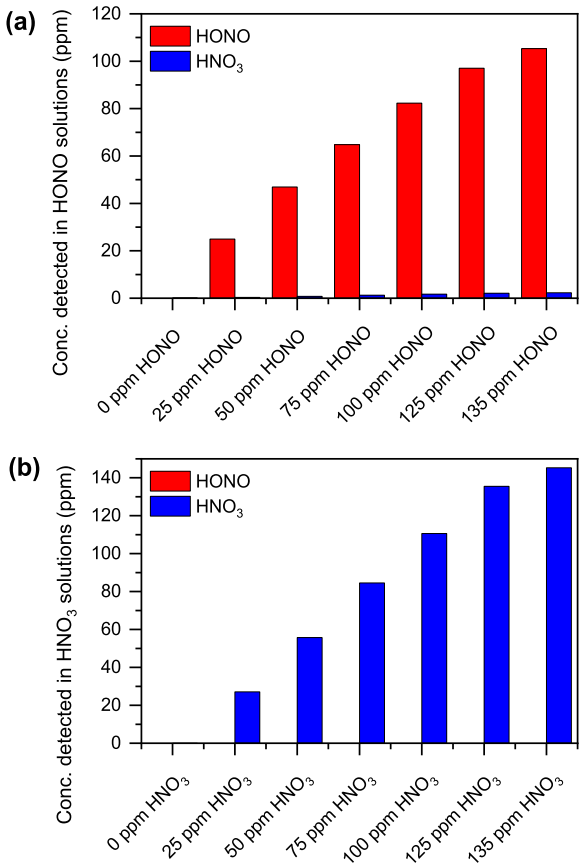

Figure 1. Control experiment: HNO_3 is produced by HONO in solution, (a) and HONO is not produced by HNO_3 in solution (b).

https://doi.org/10.1021/acsomega.3c00748
ACS Omega 2023, 8, 14730−14741

previously discussed in reactions 6 and (7), HNO_3 could also revert to HONO when it undergoes thermal decomposition[12] or when introduced to a high concentration of $NO^{\bullet}$[28] in the liquid phase.

2.2. BDNPA/BDNPF (A/F) Molarity Ratio. To understand the difference in the degree of degradation between BDNPA and BDNPF, the A/F molar ratios in air-aged and water-aged NP samples are determined, as shown in Figure 2.

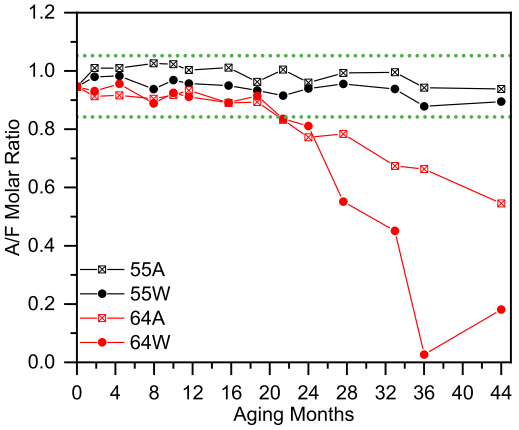

Figure 2. A/F molar ratios of air-aged and water-aged NP samples as a function of time at 55 and 64 °C. The normal range is indicated by the region between the green lines: 0.842 to 1.053.

At time zero of NP aging, the A/F molar ratio is determined at 0.947 ± 0.038. Besides measurements after 21 months at 64 °C, all A/F ratios are captured within the reported normal range between 0.842 and 1.053 (equivalent to 0.88−1.10 A/F mass ratio), as shown in the region between the green lines in Figure 2,[29] confirming that the rate of degradation in BDNPA is comparable to that in BDNPF in the early stage of thermal aging if they degrade. Even at 55 °C, the A/F molar ratio remains above 0.842. However, after 21 months at 64 °C (e.g., the late stage of NP aging), the A/F ratio plummets below 0.842 in both aging environments, which indicates a faster degradation rate of BDNPA than that of BDNPF due to the rise of acid-catalyzed hydrolysis as a dominant degradation mechanism.[15,22,30]

Using the obtained BDNPA and BDNPF concentrations, the relative abundance of HNO_x (HONO + HNO_3) in aged NP is evaluated. Prior to the occurrence of acid-catalyzed hydrolysis, the detected concentrations of HONO and HNO_3 from IC are less than 1.00 and 1.35 mM in NP, respectively. Compared to the concentration of the baseline NP (BDNPA + BDNPF, 4346 mM), the combined total of HNO_x is corresponding to less than 0.01 wt % in NP, which suggests the concentration of BDNPA/F that undergoes HONO elimination is at a trace level, yet significant seeding effect in NP aging is observed, which cannot be detected if one only uses the A/F ratio. Therefore, the high-resolution IC technique was applied to detect acidic constituents at the trace level, which should provide insight on chemistry occurring in the early stage of NP aging.

2.3. Aging in the Air Environment. *2.3.1. Air Aging at Low Temperatures.* Figure 3 presents the total concentration profiles of HONO determined in air-aged NP samples at 38 and 45 °C. In the same plot, the intensity profile of dinitro-PBNA is also included to assess its role in protecting NP from degradation in the air environment. From the IC analysis, only

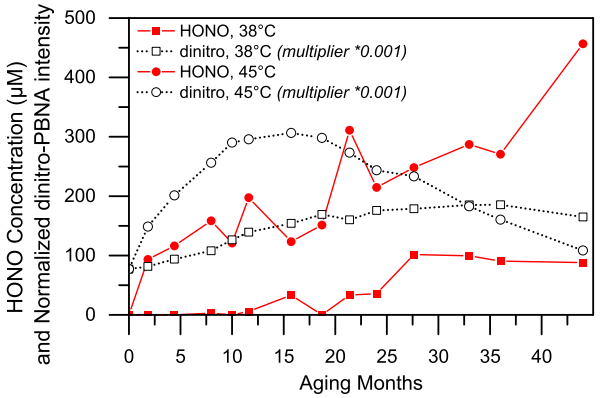

Figure 3. Time evolution of HONO in air-aged NP samples at 38 °C (red square) and 45 °C (red circle). The relative intensities of dinitro-PBNA at 38 °C (hollow square, dotted) and 45 °C (hollow circle, dotted) are obtained from a previous study[15] and normalized by a multiplier of 0.001 to best fit the magnitude of the acid concentrations (e.g., *y*-axis). Therefore, the dinitro-PBNA data are unitless and only used for qualitative comparison.

HONO is detected (Figure 3, red lines). The absence of DNPOH, acetic/formic acids, oxalic acid, and HNO_3 excludes the suspicion of NP hydrolysis. These results provide experimental evidence that HONO elimination is a primary degradation mechanism in the early stage of NP. Although the overall HONO generation is very low, the formation rates of HONO at both temperatures do exhibit a linear function of time. The overall HONO concentration after 44 months of aging is less than 0.50 mM. Since the dinitro-PBNA is not completely consumed at low temperatures, the produced $NO_2^{\bullet}$ from HONO decomposition is continuously scavenged throughout the 44 months. Therefore, the formation of HNO_3 is inhibited, and hence NP degradation is limited at the HONO elimination step and the subsequent decomposition reaction 1 during its early stage.

2.3.2. Air Aging at Elevated Temperatures. Figures 4 and 5 show the total concentration profiles of degraded NP products (e.g., acids and DNPOH) and the intensity profile of PBNA derivatives at 55 and 64 °C. The rise and fall of their concentration or intensity have demonstrated the coordinated interactions between the three reaction pathways proposed in Scheme 1. As shown in Figure 4, a faster progression of PBNA nitration is observed at 64 °C than at 55 °C, supporting the acceleration effect of temperature. Prior to the depletion of dinitro-PBNA (e.g., <28 months at 55 °C and <15 months at 64 °C), the overall concentration of HONO is less than 0.30 mM (Figure S2). Although the HONO concentration is less than what we previously observed at low temperatures (Figure 3), the presence of HNO_3, oxalic acid, acetic/formic acids, and DNPOH are detected at these high temperatures, suggesting that NP degradation has progressed beyond the HONO elimination stage. As some HONO molecules are consumed to form more degraded products, like HNO_3, oxalic acid, acetic/formic acids, and DNPOH, their estimated concentrations are below 0.30, 0.06, 2, and 4 mM, respectively. The presence of HNO_3, even at low concentrations, has led to the subsequent minor hydrolysis of NP.

The depletion of dinitro-PBNA indicates that NP aging has entered its late stage. As shown in Figures 4 and 5, in the late stage, the concentrations of all degraded species are greatly increased, on average by 30-fold in HONO, 10-fold in HNO_3,

https://doi.org/10.1021/acsomega.3c00748
ACS Omega 2023, 8, 14730−14741

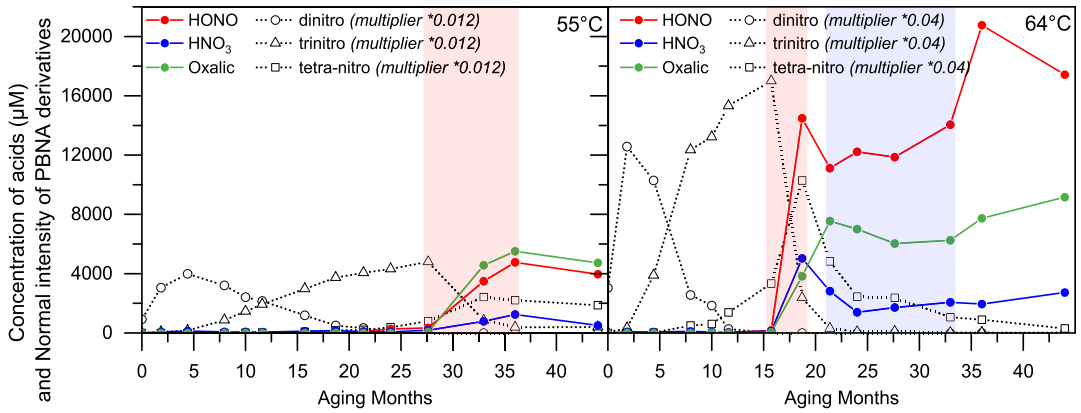

Figure 4. Time evolution of HONO, HNO_3, and oxalic acid in air-aged NP samples at 55 °C (left) and 64 °C (right). The relative intensities of dinitro- (circle, dotted), trinitro- (triangle, dotted), and tetra-nitro- (square, dotted) PBNA derivatives at 55 and 64 °C are obtained from a previous study[15] and normalized by multipliers of 0.012 and 0.04, respectively, to best fit the magnitude of the acid concentrations (e.g., *y*-axis). Therefore, the PBNA derivatives data are unitless and only used for qualitative comparison. The red columns highlight the time intervals (28−36 months at 55 °C and 15−18 months at 64 °C) when the increase of acidic components is most rapid. The blue column highlights the time interval (21−33 months at 64 °C) when the decomposition products are in the process of equilibrium adjustment.

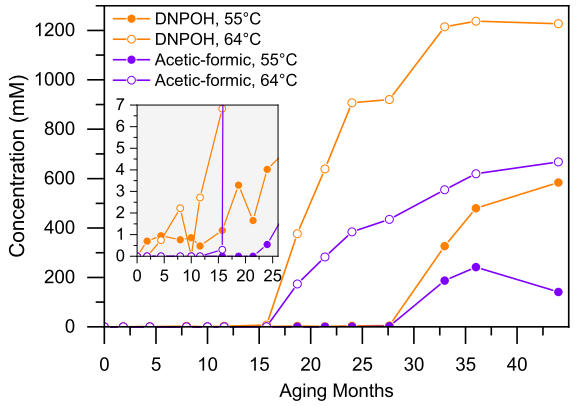

Figure 5. Time evolution of acetic/formic acids and DNPOH in air-aged NP samples at 55 and 64 °C. The inset depicts the concentration changes in the early stages of NP aging. In the late stage, the concentrations of acetic/formic acids and DNPOH generated are at least 100 times higher in magnitude than those of HONO, HNO_3, and oxalic acid.

70-fold in oxalic acid, 90-fold in acetic/formic acids, and 70-fold in DNPOH, respectively. The surge of degraded products verifies two important associations: (1) the initiation of aggressive NP hydrolysis is consequent to the depletion of dinitro-PBNA or the maximum of trinitro-PBNA, and (2) the formation of tetra-nitro derivatives is catalyzed by high acidity and high temperatures.[15]

2.3.3. Decomposition of HNO_3. In addition, a higher HONO concentration compared with HNO_3 during the late stage of NP aging is displayed in Figure 4, suggesting the chemical equilibrium favors both the production of HONO and the decomposition of HNO_3. Based on reactions 2) to 7), the enhanced rate of HONO formation can be attributed to two probable pathways: (1) the saturation of $NO^{\bullet}$ leads to HONO formation by reacting with newly formed HNO_3 (i.e., reaction 7);[28] (2) hydrogen abstraction via $NO_2^{\bullet}$[14,31] with neighboring molecules, because the antioxidant is no longer effectively scavenging these free radicals. Besides HONO decomposition, the source of $NO_2^{\bullet}$ can also be derived from the oxidation of saturated $NO^{\bullet}$ via O_2 in reaction 4 and the thermal decomposition of HNO_3 in reaction 6.[12] Additionally, the N−H moiety in tetra-nitro-PBNA should readily give off its

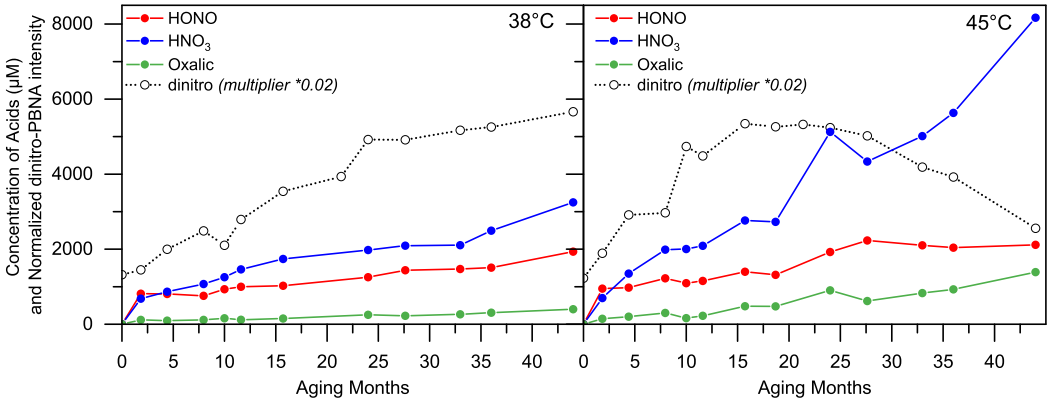

Figure 6. Time evolution of HONO, HNO_3, and oxalic in water-aged NP samples (W + WW) at 38 and 45 °C. The data are combined to visualize the overall changes in water-aged NP samples as a whole. The relative intensities of dinitro-PBNA (hollow circle, dotted) at 38 and 45 °C are obtained from previous study[15] and normalized by a multiplier of 0.02 to best fit the magnitude of acid concentrations (e.g., *y*-axis). Therefore, the dinitro-PBNA data are unitless and only used for qualitative comparison.

https://doi.org/10.1021/acsomega.3c00748
ACS Omega 2023, 8, 14730−14741

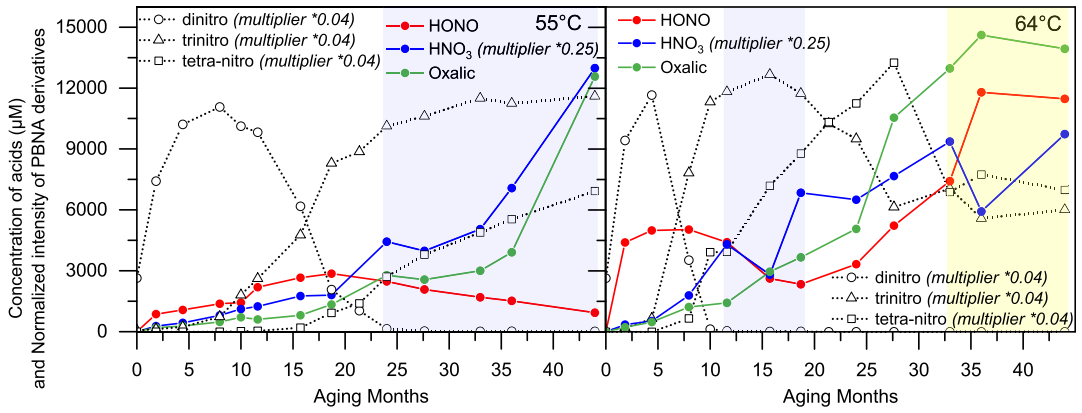

Figure 7. Time evolution of HONO, HNO_3, and oxalic acid in water-aged NP samples (W + WW) at 55 °C (left) and 64 °C (right). HNO_3 concentrations are scaled by a multiplier of 0.25 due to their high concentrations. The data are combined to visualize the overall changes in the water-aged NP samples as a whole. The relative intensities of dinitro (circle, dotted), trinitro (triangle, dotted), and tetra-nitro (square, dotted) PBNA derivatives at 55 and 64 °C are obtained from a previous study[15] and normalized by a multiplier of 0.04 to best fit the magnitude of the *y*-axis. Therefore, the PBNA derivatives data are unitless and only used for qualitative comparison. The blue and yellow columns highlight the time intervals (24−44 months at 55 °C and 12−18 months and 33−44 months at 64 °C) when the decomposition products are in the process of equilibrium adjustment.

hydrogen atom due to the destabilization caused by the four nitro groups. Together, the hydrogen abstraction and reaction 7 explain the higher HONO concentration compared with HNO_3 and the reported consumption of $NO^{\bullet}$ in the late stage of NP aging[13] as well as provide a simplistic picture for understanding NP degradation in the air environment and elevated temperatures.

2.3.4. Air-Aged Degradation Pattern. In the concentration profiles highlighted in the red and blue columns of Figure 4, the spike and plateau correspond to the processes of acid accumulation and equilibrium adjustment in the hydrolysis of NP, respectively. Inside the red columns, the increases of HONO, HNO_3, oxalic acid, and tetra-nitro-PBNA are analogous between 55 and 64 °C. Again, the TTS principle is demonstrated by the shortened time span of 3 months from 6 months with respect to the increased temperature. The subsequent plateau inside the blue column (e.g., 21 to 44 months) shows small fluctuations among the various volatile species (e.g., HONO, HNO_3, and oxalic acid), resembling a chemical equilibrium in action. Due to a decrease in the production rate of HNO_3 after 21 months at 64 °C, the formation rates of acetic/formic acids and DNPOH are also reduced (Figure 5), demonstrating that the hydrolysis of NP is slowed down during the equilibrium process. Based on the similar spike observed at 36 months at 64 °C, it is predictable that the hydrolysis of NP will progress in a consecutive rotation of spike (red column) and plateau (blue column) until all NP are decomposed. Following the logic of this pattern, one can expect that the NP hydrolysis is significantly more severe at 64 °C than at 55 °C since the first acid spike at 64 °C arrives more than 12 months earlier than that at 55 °C, as shown in Figure 4, which is also evidenced by the 2-fold difference in magnitudes (*y*-axis) of acetic/formic acids and DNPOH between 55 and 64 °C, as shown in Figure 5.

2.4. Aging in a Wet Environment. *2.4.1. Water Aging at Low Temperatures.* Figure 6 presents the total concentration profiles of HONO, HNO_3, and oxalic acid determined in both the aqueous and NP phases of water-aged NP samples at 38 (left) and 45 °C (right). In addition, the intensity profile of dinitro-PBNA is included, supporting that the dinitro-PBNA is still actively scavenging radicals formed from HONO decomposition within 44 months. The formation of HONO is a linear function with time in the wet environment (Figure 6), analogous to the trend observed in the air environment (Figure 3). After 44 months of aging, the magnitude of HONO concentration in the water-aged samples (<2.2 mM) is approximately 5 times higher than that found in the air-aged samples, owing to the encapsulation of volatiles provided by the aqueous layer, which also stabilizes the formation of HNO_3. Hence, the concentration of HNO_3 results in a linear increase with time. Consequently, low concentrations of acetic/formic acids and DNPOH are formed and estimated at less than 29 and 50 mM, respectively, despite the relatively low HNO_3 concentration. The overall amount of hydrolysis products in both phases yields a combined total of less than 0.66 wt % in the water-aged NP samples. As expected, due to the excess amount of water inside NP samples, NP hydrolysis starts at these low temperatures, though the overall NP hydrolysis is minimal thanks to the low concentration of HNO_3.

2.4.2. Water-Aged at Elevated Temperatures. The total concentration profiles determined in NP degradation products of water-aged samples at 55 and 64 °C are presented in Figures 7 and 8. In Figure 7, the intensity profiles of dinitro-, trinitro-, and tetra-nitro-PBNAs are also included to assess the changes in acidic constituents with respect to the progression of PBNA nitration. Compared to aging in the air environment (Figure 4), three noticeable differences in the water environment are observed (Figure 7): (1) the decline of HONO after the depletion of dinitro-PBNA (highlighted in the blue columns, >24 months at 55 °C and 12−18 months at 64 °C); (2) the detection of higher HNO_3 than HONO concentrations (>4-fold); and (3) the early formation of tetra-nitro-PBNA (about the same time as trinitro-PBNA). Leveraging the parallel reaction pathways proposed in Scheme 1, the association between all three events is explained. As mentioned above, particularly for the water-aged NP samples, the aqueous layer captures the decomposition products of HONO and stabilizes the produced HNO_3. Due to limited evaporation of HONO into the vapor phase and inhibited thermal decomposition of HNO_3 in a water environment (reaction 6), the production of HNO_3 is favored in the wet condition at elevated temperatures.

https://doi.org/10.1021/acsomega.3c00748
ACS Omega 2023, 8, 14730−14741

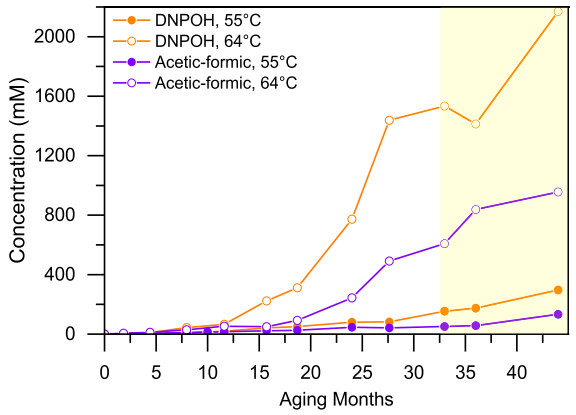

Figure 8. Time evolution of acetic/formic acids and DNPOH in water-aged NP samples at 55 and 64 °C. The data are combined to visualize the overall changes in water-aged NP samples as a whole.

However, the scavenging of free radicals by stabilizers can be a competitive reaction to the production of HNO_3 since both consume $NO_2^{\bullet}$. Therefore, the formation of HNO_3 is suppressed in the presence of dinitro-PBNA (<24 months at 55 °C). After the depletion of dinitro-PBNA, trinitro-PBNA is a much less effective stabilizer. Therefore, the production rate of HNO_3 is no longer suppressed. Upon a higher concentration (>10-fold) and faster production rate of HNO_3 in the water than in the air environment, the formation of tetra-nitro-PBNA (from trinitro-PBNA) also starts earlier and faster. Likewise, due to the excess amount of water, the magnitudes of acetic/formic acids and DNPOH concentrations are doubled in the water environment (Figure 8), indicating a faster hydrolysis rate of NP, compared to the air environment (Figure 5).

2.4.3. Water-Aged Degradation Pattern. Similar to what we have observed in the air-aged NP samples at elevated temperatures (Figure 4), the concentration profiles of degraded products found in the water-aged NP samples also exhibit a rotating pattern. As shown in Figure 7, both the blue and yellow columns show a greater fluctuation between concentrations of HONO, HNO_3, and oxalic acid than those found in the nonhighlighted regions, which resembles the process of equilibrium adjustment observed in the air-aged NP samples (Figure 4, blue column), but at a shorter duration (i.e., 6 months in water-aged vs 12 months in air-aged at 64 °C), and it fluctuates to a greater extent (i.e., sharp decrease in HNO_3). On the other hand, the nonhighlighted region shows a gradual increase of acidic components until their maximum is reached, similar to the spike observed in the air-aged NP sample (Figure 4, red column), except at a longer duration (i.e., 15 months in water-aged vs 3 months in air-aged at 64 °C) and at a slower rate. Additionally, as highlighted in the yellow columns in Figures 7 and 8, an inverse correlation between the concentration changes in HONO and oxalic acid and those in HNO_3 and DNPOH is observed, suggesting these four species are perhaps the key components involved in the equilibrium adjustment process. Compared to the air environment, the disparity between 55 and 64 °C is even greater in the water environment—a difference of one full cycle (At 55 °C: first acid spike → first equilibrium; At 64 °C: first acid spike → first equilibrium → second acid spike → second equilibrium), which is also evidenced by the 7-fold difference in magnitudes (y-axis) of acetic/formic acids and DNPOH between 55 and 64 °C. As expected, the key difference between the air and water conditions is the excess amount of water, which creates three contradictory effects: (1) to hinder HONO formations through reactions 1, 5 and HNO_3 formation through reaction 5; (2) to reduce acidity through HNO_3 extraction and water dilution; and (3) to hydrolyze NP once the acidity is above the threshold.

2.5. DNPOH-to-Acetic/Formic Acid Ratio. In both water-aged and air-aged samples, when acid-catalyzed hydrolysis progresses aggressively (e.g., after depletion of dinitro-PBNA), a strong positive correlation is found between the molarities of acetic/formic acids and DNPOH at a Pearson constant above 0.95 and at a very low p-value (10^{-6}), as shown in Figure 9. The slopes of 2.125 and 2.310 suggest the

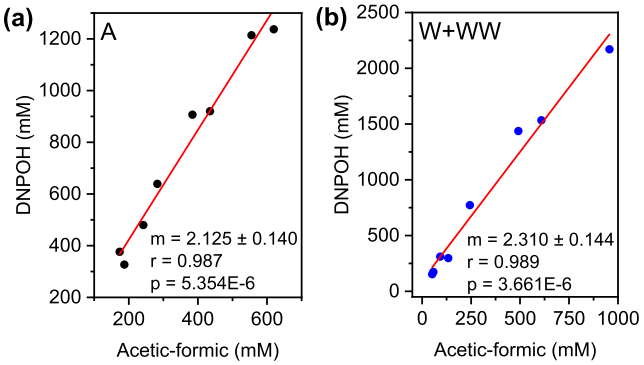

Figure 9. Correlation between DNPOH and acetic/formic acids gives a 2:1 ratio at high concentrations of HNO_x and water. The analyzed data are extracted from the selected aging periods after the depletion of dinitro-PBNA and the maximum of trinitro-PBNA. For air-aged NP samples(A) in (a), the selected periods include 33 to 36 months at 55 °C and 18 to 36 months at 64 °C. For wet-aged NP samples (W + WW) in (b), the selected periods include 33 to 44 months at 55 °C and 18 to 44 months at 64 °C.

production ratio of DNPOH-to-acetic/formic acids is approximately 2:1, which matches the stoichiometry of **4b** and **5b** proposed in Scheme 1. Given the values after the decimal points, the discrepancies of 0.125 and 0.310 can be attributed to the high volatility of acetaldehyde and formaldehydes.

2.6. Aqueous and NP Phases in Water-Aged Samples. *2.6.1. Degradation Gradient.* Since aging NP in direct contact with water is quite different from the ordinary aging condition where NP has been used, by preventing the volatiles from escaping into the vapor phase, we managed to obtain additional insights into the degradation mechanism of NP. As discussed in Table 1, the decomposition product profile is composed of diverse chemicals with different densities and solubilities. Due to the partitioning of chemicals between the aqueous (WW) and NP (W) phases in the water-aged samples, three distinctive regions are created, as indicated by the arrows in Figure 10. To evaluate this partitioning effect, the concentration profiles in the water-aged samples at low and elevated temperatures are separated by their corresponding phases, as displayed in Figures 11 and 12.

The water-soluble products are mostly extracted into the aqueous phase, including HNO_3 and oxalic and acetic/formic acids, as shown in Figures 11B1,C1,D1 and 12B1,C1,D1. As highlighted in the green columns of Figure 12A2,B1,B2, the exchange of HONO and HNO_3 is most pronounced at 64 °C (blue, solid circle) between 15 and 24 months, which is

https://doi.org/10.1021/acsomega.3c00748
ACS Omega 2023, 8, 14730−14741

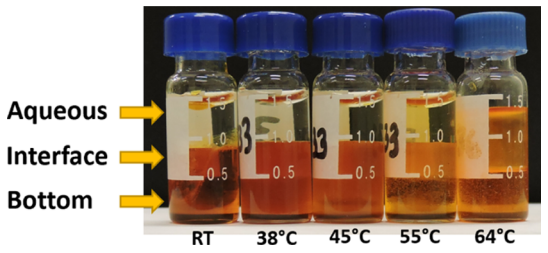

Figure 10. Three regions of degradation in 36 month (samples were incorrectly labeled as 33 months) aged NP samples in the wet environment at various temperatures.

reflected by the troughs of HONO and HNO_3 in the NP phase and the increase of HNO_3 in the aqueous phase. Due to the accelerated diffusion rate at elevated temperatures, HONO is lost, and HNO_3 production is minimized in the NP phase, resulting in the observed troughs in Figure 12A2,B2. As more HONO molecules are captured at the interface, they can decompose into HNO_3, which is extracted into the aqueous phase, resulting in a sharp increase of HNO_3 observed in Figure 12B1. In the presence of high HNO_3 concentration, NP or DNPOH can be decomposed into CO, CO_2, and acetic/formic acid components and thus converted to oxalic acid. Due to the accumulation of highly soluble acids, the color of the aqueous phase changes from clear to amber with increasing temperatures, while the color of the NP phase lightens (Figure 10).

Conversely, the decomposition products with poor solubility in water are mostly retained in the NP phase, including HONO and DNPOH, as shown in Figures 11A2,E2 and 12A2,E2. The retention of HONO in the NP phase is mainly due to its poor water solubility, as previously noted. Interestingly, some DNPOH is extracted into the aqueous phase, as indicated in Figures 11E1 and 12E1. The distribution of DNPOH between aqueous and NP phases varies at different temperatures: 100% (<6 mM), 33% (<12 mM), 11% (<30 mM), and 5% (<100 mM) in the aqueous phase at 38, 45, 55, and 64 °C, respectively. The increased solubility of DNPOH in the aqueous phase can be explained by two facts: (1) DNPOH as an alcohol, and (2) an increased in acidity. First of all, compared to the BDNPA/F, the solubility of DNPOH in water is improved by its hydroxyl group (i.e., hydrogen bonding with water). Secondly, the increased acidity in the aqueous phase and interface enhances the solubility of DNPOH, which explains why a trace amount of DNPOH can be completely extracted into the aqueous phase at 38 °C. At elevated temperatures, the acidity is further increased, and more DNPOH is formed, which therefore increases the amount of DNPOH dissolved in the aqueous phase. Nevertheless, the expressed percentage with respect to the total DNPOH concentration in the aqueous phase decreases as temperature increases; this is because the partition of DNPOH is still dominated by a downward mass transport process due to its high density (1.483 g/cm^3 at 25 °C), limited solubility in water, and NP-like polarity in NP.

It is worth noting that the assimilation of the two phases is observed at 64 °C after 36 months of aging, as indicated by their similar coloration in the far-right vial in Figure 10, which decreases the volume in the NP phase and increases the volume in the aqueous phase. The decrease in total volume is likely attributed to sample loss during the aging experiment. Some volatiles could have escaped from the aging containers through a severely damaged cap. The total mass loss might also contribute to the uncertainty of the results obtained at 36 months and after.

2.7. Partial Hydrolysis. Due to its proximity to HNO_3 in the aqueous phase, partial hydrolysis of NP at the interface is highly possible in the early stage of NP aging under the wet condition. Therefore, the ratio profile of DNPOH-to-acetic/formic acids determined in the water-aged samples at 38 °C is examined during this period of time. As shown in Figure 13,

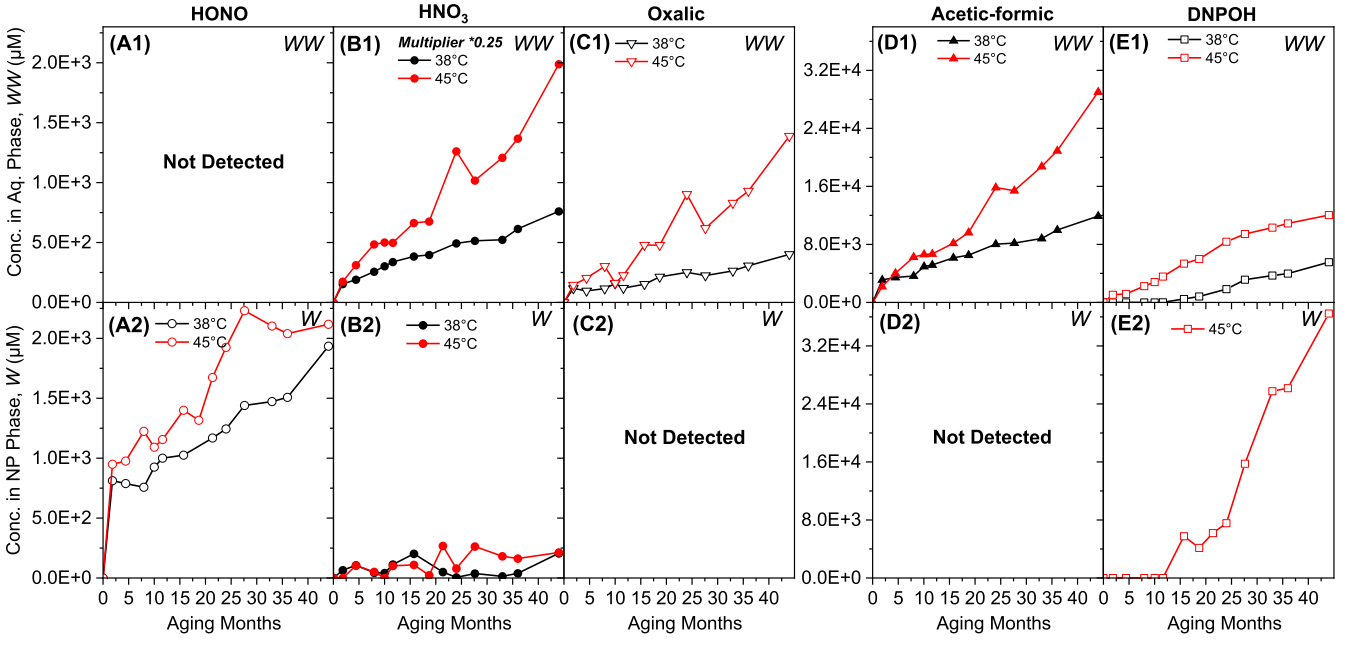

Figure 11. Time evolution of HONO (A1,A2), HNO_3 (B1,B2), oxalic acid (C1,C2), acetic/formic acids (D1,D2), and DNPOH (E1,E2) in water-aged samples at 38 °C (black) and 45 °C (red): top row (aqueous phase, WW) and bottom row (NP phase, W). HNO_3 is mainly found in the aqueous phase (WW), plot B1, and its concentrations are scaled by a multiplier of 0.25. Besides B1, all other plots in this figure are not scaled.

https://doi.org/10.1021/acsomega.3c00748
ACS Omega 2023, 8, 14730−14741

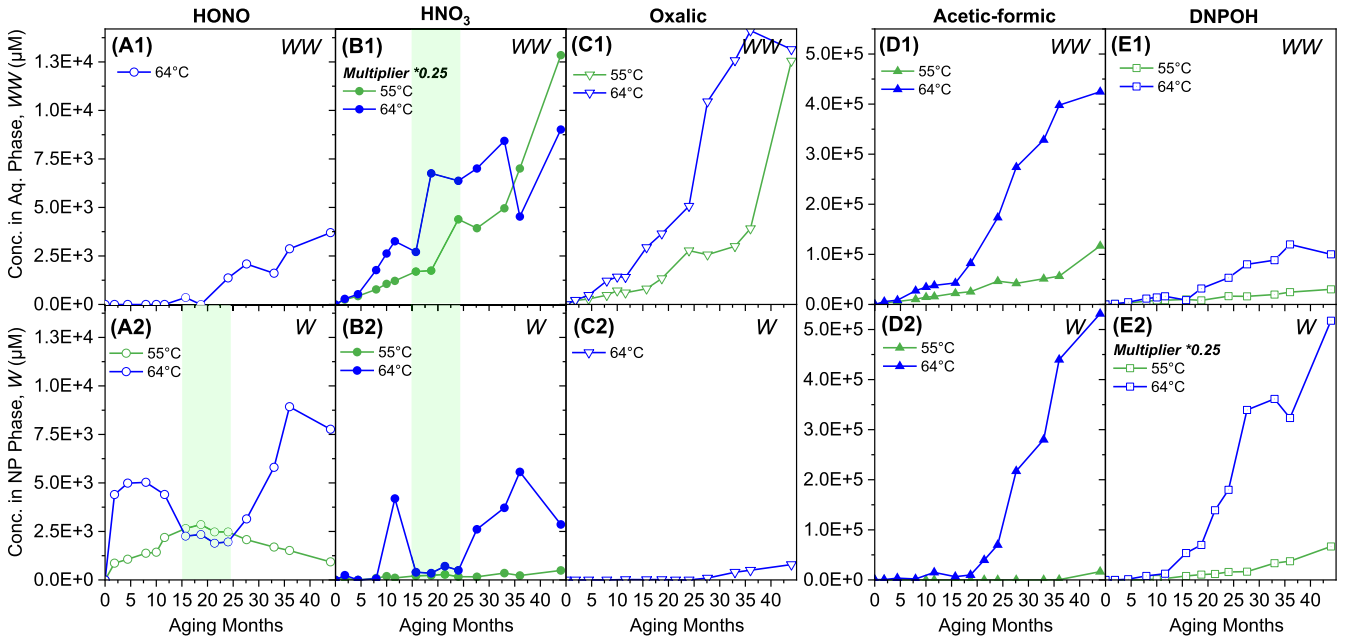

Figure 12. Time evolution of HONO (A1,A2), HNO_3 (B1,B2), oxalic acid (C1,C2), acetic/formic acids (D1,D2), and DNPOH (E1,E2) in water-aged NP samples at 55 and 64 °C: the top row (aqueous phase, WW) and the bottom row (NP phase, W). HNO_3 in the aqueous layer (WW), plot B1, are scaled by a multiplier of 0.25, indicating that HNO_3 is mainly found in the aqueous phase. DNPOH is mainly found in the NP phase (W), plot E2, and its concentrations are scaled by a multiplier of 0.25. Besides B1 and E2, all other plots in this figure are not scaled.

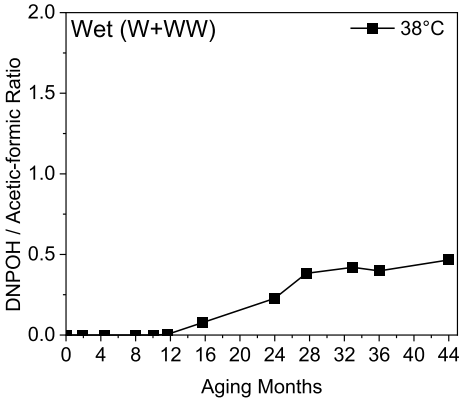

Figure 13. Ratio profile of DNPOH-to-acetic/formic acids in water-aged NP samples across 44 months at 38 °C.

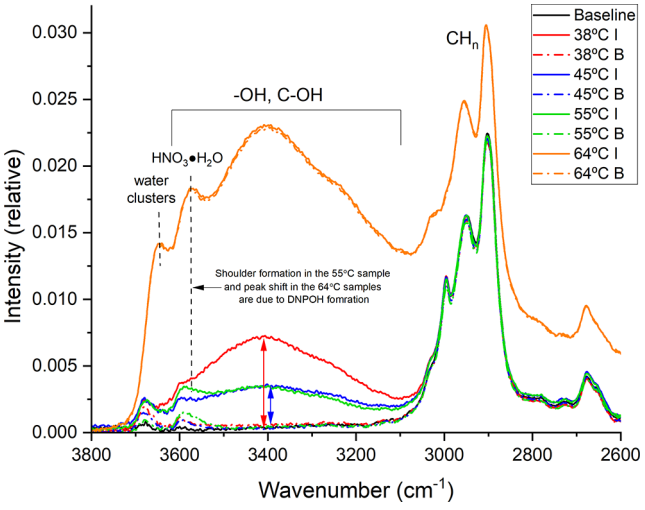

Figure 14. FTIR spectra of the interface (I) and bottom (B) regions of 36 month-aged NP samples in water environment at various temperatures.

although this ratio does increase with time after 12 months of aging, it is less than 2, which does not match the stoichiometry of **4b** and **5b** in Scheme 1. Apparently, partial hydrolysis of NP has taken place. To verify this proposition, FTIR characterization was conducted. The different FTIR spectra of the samples collected from the interface (I) and bottom (B) regions are provided for the samples aged for 36 months at various temperatures, as shown in Figure 14. While the FTIR spectrum of the B sample is more or less the same as baseline NP, the FTIR spectrum of the I sample shows significant change at temperatures below 55 °C. As the IC results suggest (see Figure 6), the overall acidity is low at 38 °C even after 44 months of aging. At such a low acidity, while a small shoulder of HNO_3 peak is observed at ∼3600 cm^{-1} in Figure 14, the increased intensity of the broad −OH/C−OH band at ∼3400 cm^{-1} is likely associated with **2b** (Scheme 1), which confirms the partial hydrolysis of NP. At 55 °C and above, the shoulder at ∼3600 cm^{-1} grows into a peak, shifts to ∼3580 cm^{-1}, and is even more evidenced at 64 °C, due to the increased acidity in the aged NP samples (see Figure 7). At higher acidity, NP can hydrolyze into smaller molecules. Therefore, the viscosity of the aged sample decreases,[22,32] which is responsible for the greatly increased intensity of CH_n bands (2900−3000 cm^{-1}). The largely grown −OH/C−OH band in the 64 °C sample is likely associated with the formation of DNPOH because 1 mol of BDNPA could yield 2 mol of DNPOH as NP hydrolysis progresses into the late stage, as shown in Scheme 1. Furthermore, the regional difference is found to be the most significant at 38 °C and eventually diminishes at 64 °C, suggesting that temperature increases reactivity and acidity in the NP phase and hence the miscibility between the different regions. Based on the agreements shown between the FTIR, liquid chromatography coupled with quadrupole time-of-flight

https://doi.org/10.1021/acsomega.3c00748
ACS Omega 2023, 8, 14730−14741

mass spectrometry (LC−QTOF), and IC results, we conclude that the NP degradation is limited within the reactions of elimination and decomposition of HONO and the partial hydrolysis of the NP when it is aged at 38 °C for 44 months in a water environment.

2.8. HNO_3 Threshold. Following the confirmation of partial hydrolysis, we proceed to determine the HNO_3 threshold, which marks the initiation of NP hydrolysis. The starting point of NP hydrolysis (e.g., partial hydrolysis) in the air-aged and the water-aged NP samples are compared, as shown in Table 2. In the air-aged samples (Figure 4), while

Table 2. Detected Degradation Products in the Aqueous Samples (WW) at Various Temperatures

temperature (°C)	aging months	HONO (μM)	HNO_3 (μM)	DNPOH (mM)
38	2	0	615	0
38	12	0	1350	0.02
45	2	0	697	1.05
55	2	0	1016	1.16
64	2	0	1171	1.32

partial hydrolyzation is observed between 2 and 28 months at 55 °C and between 2 and 15 months at 64 °C, due to the evaporation of volatiles into the vapor phase, particularly HONO, and possible thermal decomposition of HNO_3, the results from the air-aged samples cannot accurately determine the HNO_3 threshold of NP hydrolysis. However, assuming the evaporation of volatiles is minimal in ordinary storage conditions (<38 °C), the water and HNO_3 are perhaps preserved within the NP phase, meaning there will be a slow and linear accumulation rate of the acidic constituents, and the resulting trends may be similar to those presented in Figure 6. Therefore, the results of the aqueous samples (Table 2) are likely the most suitable dataset to estimate the HNO_3 threshold for the initiation of partial hydrolysis. After 2 months at 38 °C, partial hydrolysis of NP is not observed despite the concentration of HNO_3 being comparable to the 2 month sample at 45 °C, which demonstrates the influence of higher temperature in accelerating the hydrolysis of NP. Given the 12 month aqueous sample in Table 2, twice the concentration of HNO_3 is required for partial hydrolysis to happen at 38 °C. Hence, it is safe to assume NP is not hydrolyzed as long as the HNO_3 concentration is maintained below 1.35 mM and below 38 °C.

3. CONCLUSIONS

Rapid, reproducible, and direct determination of HONO, HNO_3, acetic/formic acids, and oxalic acid is achieved by leveraging a simple LLE technique with IC capability. The IC results confirm HONO generation and support HONO elimination as an initial reaction in NP degradation. Most importantly, HONO conversion to HNO_3 is the key factor for inducing the acid-catalyzed hydrolysis of NP in the later stage of NP degradation. Since HONO is a highly unstable species and has poor solubility in water, the measurement of HONO may present high uncertainty, and thus, it is impossible to use it as a quality control of NP. On the other hand, HNO_3 concentration evaluation can provide a better assessment of early NP degradation to avoid the risk of acetal/formal hydrolyzation. Additionally, the effect of temperature should be considered for the monitoring process since elevated temperatures will lead to a faster formation rate of HONO (via elimination) and the subsequent complex autocatalytic reactions of small molecules (e.g., reactions 1−8), which ultimately increase the acidity of aged NP samples and hence NP hydrolysis. Overshadowed by the acidity of baseline carboxylic acids, typical evaluations such as AN cannot detect the trace-level changes in HNO_3 (μM). Instead, the developed method in the current study evaluates acidic constituents with much higher specificity. Using the determined HNO_3 threshold (1.35 mM below 38 °C), we can precisely monitor the initiation and progression of NP degradation. Future studies will focus on the design of remediation and appropriate control of the HNO_x concentration in aged NP.

4. EXPERIMENTAL SECTION

4.1. Materials. BDNPA/F standards were provided by CNS Pantex Plant (Amarillo, Texas). The baseline NP was obtained from a newly opened drum stored at the Los Alamos National Laboratory, which passed industry standard qualification tests upon opening. Though this material is more than 50 years old, it is referred to as the baseline NP because all aged samples were prepared from this material. DNPOH was synthesized by David Langlois at the Los Alamos National Laboratory.[33] Reference standards of fluoride, chloride, nitrite, sulfate, acetate, oxalate, bromide, nitrate, and phosphate were purchased from SPEX CertiPrep (Metuchen, NJ). DI water, LC/MS grade water, and organic solvents were purchased from Fisher Chemical (Fair Lawn, NJ).

4.2. Sample Preparation. In the thermal aging experiment, the baseline NP samples were aged from 0 to 44 months at four temperatures (38, 45, 55, and 64 °C) sealed in air (air-aged) or in contact with deionized (DI) water (water-aged).[22,23,34] The air-aged samples are solely composed of the baseline NP in air (A). The water-aged samples are composed of two sampling layers with a 2:1 volume ratio: 1 mL of the baseline NP at the bottom (W) and 0.5 mL of DI water as the aqueous layer on top (WW) for capturing volatile species.[22,23,33]

A total of five sample sets were prepared for analyses by IC and LC−QTOF: two sets from the air-aged NP, one set from the aqueous layer, and two final sets from the NP layer in the water-aged NP. For the aqueous layer, called aqueous sample hereinafter, a 20 μL aliquot was diluted with 980 μL of LC/MS grade water using digital pipettes (<1% error in precision and accuracy). Due to the poor solubility of NP in water and the fact that the IC instrument cannot run organic solvents, NP samples were prepared separately as organic and aqueous extracts for LC-QTOF and IC, respectively; therefore, the entire NP degradation profiles were captured. The organic extracts were obtained by dissolving 3.0 ± 0.5 mg of the aged NP in 10 mL of acetonitrile. To prepare for the aqueous extracts, a new extraction method was developed as follows: three repeated LLEs with 1.5 mL of water on 20.0 ± 1.0 mg of aged NP. In each LLE, the vortex mixer was set to 3000 rpm for 15 s, and the particulates were allowed to settle for 1−5 min. Then, the aqueous extracts are collected and combined to a final volume of 4.5 mL. Using this developed LLE method, the extraction efficiencies are estimated to be 100% in HNO_3 and oxalic acid, 50% in HONO, and 59% in acetic/formic acids. By testing this method in baseline NP, 4 month, and 28 month air-aged samples at 55 °C, the triplicate results show a standard error of measurements at 11%.

https://doi.org/10.1021/acsomega.3c00748
ACS Omega 2023, 8, 14730−14741

4.3. LC−QTOF and FTIR Measurements. A SCIEX X500R QTOF system coupled with an ExionLC AC was operated for negative electrospray ionization (ESI^-) and information-dependent acquisition (IDA). Concentrations of BDNPA/F and DNPOH were determined using calibration ranges of 90−240 and 2−80 ppm, respectively. The detailed analytical method is described in our previous works.[15,16] A Thermo Nicolet iS50 FTIR spectrometer was used to conduct the FTIR measurement in the attenuated total reflectance mode between 4000 and 450 cm^{-1}. A diamond crystal was used. The spectra were collected at 4 cm^{-1} resolution with 32 scans. Prior to the measurement, the FTIR instrument was purged under N_2 for at least 2 h to ensure baseline stability. For the water-aged NP, the spectra were collected for both the aqueous and NP phases.[22,23]

4.4. IC Measurements. The separation of anions in the sample was done on a Dionex ICS-2100 instrument (Thermo Fisher Scientific Inc., USA) following EPA Method 300.0.[35] The column is a Dionex IonPac AS15 (Thermo Scientific, Waltham, MA, Prod. #053941). Mobile phase is made using an Eluent Generator Cartridge, Dionex ECG III KOH RFIC (Thermo Scientific, Waltham, MA, Prod. #074532) at a 38 mM KOH concentration using DI water with a flow rate of 0.4 mL/min. The IC system has a conductivity detector. Undiluted and 1:10 diluted samples using DI water obtained from the MilliQ system were analyzed. Complete chromatographic resolutions cannot be achieved between formate and acetate ions[36] due to column limitations; thus, both ions are combined as a sum and denoted as acetic/formic acids. The concentrations of HONO, HNO_3, acetic/formic acids, and oxalic acid were quantified using their anionic forms. The calibration standards include nitrite (0.5−5.0 ppm), nitrate (2.0−20.0 ppm), oxalate (0.5−5.0 ppm), and acetate (0.1−1.0 ppm).

Blank and time zero (e.g., baseline NP) measurements are applied as background or interference corrections to all IC results. In the first correction, values obtained from method blanks (e.g., extraction without adding the NP sample) were subtracted from the raw concentrations (in ppm) to remove potential impurities and contaminations found in water. Following the blank subtraction, HONO at 137 ± 23 μM, acetic/formic acids at 8 ± 1 mM, and oxalic acid at 59 ± 7 μM were determined in the baseline NP. Since the baseline NP is more than 50 years old, some amount of degradation products are expected. These obtained values of the baseline NP are then utilized as the second correction by performing a time zero subtraction. Therefore, we can examine the concentration changes that are exclusively related to the aging experiment, which simplifies result interpretation. Finally, to evaluate the conversion between HONO and HNO_3, a control experiment was conducted at ambient temperature using pure aqueous solutions of HONO and HNO_3 at concentrations of 0 to 135 ppm.

■ ASSOCIATED CONTENT

Supporting Information

The Supporting Information is available free of charge at https://pubs.acs.org/doi/10.1021/acsomega.3c00748.

HONO elimination model; acid concentration profiles of air-aged NP samples at 55 and 64 °C in the early stage of NP aging; and assessment of hydrochloric, hydrofluoric, and sulfuric acids (PDF)

■ AUTHOR INFORMATION

Corresponding Author

Dali Yang − *MST-7: Engineered Materials Group, Materials Science and Technology Division, Los Alamos National Laboratory, Los Alamos, New Mexico 87545, United States;* orcid.org/0000-0003-4887-6717; Email: dyang@lanl.gov

Authors

Kitmin Chen − *MST-7: Engineered Materials Group, Materials Science and Technology Division, Los Alamos National Laboratory, Los Alamos, New Mexico 87545, United States;* orcid.org/0000-0002-1869-7147

Alexander S. Edgar − *MST-7: Engineered Materials Group, Materials Science and Technology Division, Los Alamos National Laboratory, Los Alamos, New Mexico 87545, United States;* orcid.org/0000-0002-9719-3683

Zheng-Hua Li − *EES-14: Earth System Observations Group, Earth and Environmental Sciences Division, Los Alamos National Laboratory, Los Alamos, New Mexico 87545, United States;* orcid.org/0000-0003-0946-500X

Oana C. Marina − *EES-14: Earth System Observations Group, Earth and Environmental Sciences Division, Los Alamos National Laboratory, Los Alamos, New Mexico 87545, United States*

Complete contact information is available at: https://pubs.acs.org/10.1021/acsomega.3c00748

Notes

The authors declare no competing financial interest.

■ ACKNOWLEDGMENTS

The authors are grateful to Justine Yang, Jillian O'Neel, Joseph Torres, and Camille Wong for their experimental work preceding this publication. The authors would also like to thank David Langlois for the synthesis of DNPOH; Phil Leonard, Paul Peterson, Chris Freye, and Chris Snyder for their communication on acetal/formal hydrolysis in BDNPA/F; and Kevin Morris at Pantex for his parallel work on NP evaluation. This work was supported by the US Department of Energy through the Los Alamos National Laboratory Aging and Lifetimes Program. Los Alamos National Laboratory is operated by Triad National Security, LLC, for the National Nuclear Security Administration of the U.S. Department of Energy (contract no. 89233218NCA000001).

■ REFERENCES

(1) Martín-Martínez, J. M.; Fernández-Garcia, J. C.; Orgilés-Barceló, A. C. Chapter 13—Rubber base adhesives. In *Adhesion Science and Engineering*; Dillard, D. A., Pocius, A. V., Chaudhury, M., Eds.; Elsevier Science B.V.: Amsterdam, 2002; pp 573−675.

(2) Wypych, G. Chapter 3—Typical Methods OF Quality Control of Plasticizers. In *Handbook of Plasticizers*, 2nd ed.; William Andrew Publishing: Boston, 2012; pp 85−109.

(3) Désilets, S.; Villeneuve, S. Trace Determination of Strong Acids in NitroPlasticizers. *Analyst* **1997**, *122*, 995−998.

(4) Melius, C. F.; Piqueras, M. C. Initial Reaction Steps in the condensed-phase decomposition of propellants. *Proc. Combust. Inst.* **2002**, *29*, 2863−2871.

(5) Pauler, D. K.; Henson, N. J.; Kress, J. D. A mechanism for the decomposition of dinitropropyl compounds. *Phys. Chem. Chem. Phys.* **2007**, *9*, 5121−5126.

(6) Chislett, M.; Guo, J.; Bond, P. L.; Yuan, Z. Structural changes in model compounds of sludge extracellular polymeric substances caused by exposure to free nitrous acid. *Water Res.* **2021**, *188*, 116553.
(7) Chislett, M.; Yu, Z.; Donose, B. C.; Guo, J.; Yuan, Z. Understanding the Effect of Free Nitrous Acid on Biofilms. *Environ. Sci. Technol.* **2022**, *56*, 11625−11634.
(8) Zahedi, S.; Icaran, P.; Yuan, Z.; Pijuan, M. Assessment of free nitrous acid pre-treatment on a mixture of primary sludge and waste activated sludge: Effect of exposure time and concentration. *Bioresour. Technol.* **2016**, *216*, 870−875.
(9) Trache, D.; Tarchoun, A. F. Stabilizers for nitrate ester-based energetic materials and their mechanism of action: a state-of-the-art review. *J. Mater. Sci.* **2017**, *53*, 100−123.
(10) Park, J. Y.; Lee, Y. N. Solubility and decomposition kinetics of nitrous acid in aqueous solution. *J. Phys. Chem* **1988**, *92*, 6294−6302.
(11) Chlistunoff, J.; Ziegler, K. J.; Lasdon, L.; Johnston, K. P. Nitric/Nitrous Acid Equilibria in Supercritical Water. *J. Phys. Chem. A* **1999**, *103*, 1678−1688.
(12) Robertson, G. D., Jr.; Mason, D. M.; Corcoran, W. H. The Kinetics of the Thermal Decomposition of Nitric Acid in the Liquid Phase. *J. Phys. Chem* **1955**, *59*, 683−690.
(13) Salazar, M. R.; Kress, J. D.; Lightfoot, J. M.; Russel, B. G.; Rodin, W. A.; Woods, L. Experimental Study of the Oxidative Degradation of PBX 9501 and its Components. *Propellants, Explos., Pyrotech.* **2008**, *33*, 182−202.
(14) Jellinek, H. H. G.; Wang, T. J. Y. Reaction of nitrogen dioxide with linear polyurethane. *J. Polym. Sci., Polym. Chem. Ed.* **1973**, *11*, 3227−3242.
(15) Chen, K.; Edgar, A. S.; Jung, J.; Kress, J. D.; Wong, C. H.; Yang, D. Liquid Chromatography Quadrupole Time-of-Flight Mass Spectrometry Analysis of Eutectic Bis(2,2-dinitropropyl) Acetal/Formal Degradation Profile: Nontargeted Identification of Antioxidant Derivatives. *ACS Omega* **2022**, *7*, 35316−35325.
(16) Chen, K.; Edgar, A. S.; Wong, C. H.; Yang, D. Liquid Chromatography Quadrupole Time-of-Flight Mass Spectrometry: A Strategy for Optimization, Characterization, and Quantification of Antioxidant Nitro Derivatives. *ACS Omega* **2022**, *7*, 32701−32707.
(17) Clayden, J.; Greeves, N.; Warren, S., Chapter 11 - Nucleophilic Substitution at C=O with Loss of Carbonyl Oxygen; Chap 39—Determining Reaction Mechanisms. *Organic Chemistry*, 2nd ed.; Oxford University Press: 2012; pp 223−228, 1058−1059.
(18) Leonard, P. W. *Mechanism of acetal (or formal) hydrolysis (Personal Communication)*; Los Alamos National Laboratory: Los Alamos, NM, United States, 2016.
(19) Kress, J. D. *Nitroplasticizer Resistance to Hydrolysis (Personal Communication)*; Los Alamos National Laboratory: Los Alamos, NM, United States, 2006.
(20) Freye, C. E.; Snyder, C. J. Investigation into the Decomposition Pathways of an Acetal-Based Plasticizer. *ACS Omega* **2022**, *7*, 30275−30280.
(21) Rana, M. S.; Guzman, M. I. Oxidation of Catechols at the Air-Water Interface by Nitrate Radicals. *Environ. Sci. Technol.* **2022**, *56*, 15437−15448.
(22) Yang, D.; Edgar, A. S.; Torres, J. A.; Adams, J. C.; Kress, J. D. Thermal Stability of a Eutectic Mixture of Bis(2,2-dinitropropyl) Acetal and Formal: Part C. Kinetic Compensation Effect. *Propellants, Explos., Pyrotech.* **2020**, *46*, 134−149.
(23) Yang, D.; Zhang, D. Z. Role of water in degradation of nitroplasticizer. *Polym. Degrad. Stab.* **2019**, *170*, 109020.
(24) Guzman, M. I.; Martin, S. T. Photo-production of lactate from glyoxylate: how minerals can facilitate energy storage in a prebiotic world. *Chem. Commun.* **2010**, *46*, 2265−2267.
(25) Schuler, E.; Demetriou, M.; Shiju, N. R.; Gruter, G. M. Towards Sustainable Oxalic Acid from CO(2) and Biomass. *ChemSusChem* **2021**, *14*, 3636−3664.
(26) pK_a Data Compiled by R. Williams, W.P. Jencks, F.H. Westheimer; Updated 4/7/2022. ACS, Organic Division: 2022.
(27) Eugene, A. J.; Pillar-Little, E. A.; Colussi, A. J.; Guzman, M. I. Enhanced Acidity of Acetic and Pyruvic Acids on the Surface of Water. *Langmuir* **2018**, *34*, 9307−9313.
(28) Lewis, G. N.; Edgar, A. The Equilibrium Between Nitric Acid, Nitrous Acid and Nitric Oxide. *J. Am. Chem. Soc.* **1911**, *33*, 292−299.
(29) Morris, K. D. *Aged Nitroplasticizer Evaluation; PXRPT 22-01; CNS, LLC*; Pantex Plant: Amarillo, TX, USA, March 1, 2022.
(30) Yang, D.; Pacheco, R.; Edwards, S.; Torres, J.; Henderson, K.; Sykora, M.; Stark, P.; Larson, S. Thermal stability of a eutectic mixture of bis(2,2-dinitropropyl) acetal and formal: Part B. Degradation mechanisms under water and high humidity environments. *Polym. Degrad. Stab.* **2016**, *130*, 338−347.
(31) Pryor, W. A.; Lightsey, J. W. Mechanisms of Nitrogen Dioxide Reactions: Initiation of Lipid Peroxidation and the Production of Nitrous Acid. *Science* **1981**, *214*, 435−437.
(32) Yang, D.; Pacheco, R.; Edwards, S.; Henderson, K.; Wu, R.; Labouriau, A.; Stark, P. Thermal stability of a eutectic mixture of bis(2,2-dinitropropyl) acetal and formal: Part A. Degradation mechanisms in air and under nitrogen atmosphere. *Polym. Degrad. Stab.* **2016**, *129*, 380−398.
(33) Edgar, A. S.; Wong, C. H.; Chen, K.; Langlois, D. A.; Yang, D. Identification of 2,2-dinitropropanol, a Hydrolyzed Product of Aged Eutectic Bis(2,2-dinitropropyl) Acetal − Bis(2,2-dinitropropyl) Formal Mixture. *Propellants, Explos., Pyrotech.* **2022**, *47*, No. e202100345.
(34) Wong, C. H.; Edgar, A. S.; Yang, D. Liquid Chromatography Mass Spectrometry Study of a Eutectic Mixture of bis(2,2-Dinitropropyl) Acetal/Formal. *Propellants, Explos., Pyrotech.* **2021**, *46*, 1849−1859.
(35) Pfaff, J. D. *EPA Method 300.0: Determination of Inorganic Anions by Ion Chromatography*. Revision 2.1; U.S. Environmental Protection Agency: Cincinnati, OH, 1993.
(36) Balcerzak, M.; Kapica, D. Fast Ion Chromatographic Method for the Determination of Formates in Alcoholic Drinks. *Food Anal. Methods* **2017**, *10*, 2358−2364.

https://doi.org/10.1021/acsomega.3c00748
ACS Omega 2023, 8, 14730−14741